Structure and electronic properties of amorphous WO_3

G. A. de Wijs and R. A. de Groot
Electronic Structure of Materials, Research Institute of Materials, Faculty of Sciences, Toernooiveld 1, NL-6525 ED Nijmegen, The Netherlands

(Received 14 May 1999; revised manuscript received 27 July 1999)

The structure and electronic structure of amorphous WO_3 were studied with first-principles density-functional calculations. Upon amorphization, a large increase of the band gap is observed. The empty states exhibit a tendency towards localization. We studied the filling of these states as induced by addition of an alkali metal (Na) or removal (''deficiency'') of O. Na addition does not affect the structure much, and results in a filling of the lower part of the conduction-band continuum. Oxygen removal can induce large structural relaxations, which can give rise to the formation of W-W dimers (bond length <3.0 Å) and corresponding in-gap states. We suggest a reinterpretation of the nature of the active species in the intervalence charge-transfer mechanism that is believed to explain the electrochromic behavior of thin-film amorphous tungsten bronzes. [S0163-1829(99)12847-9]

I. INTRODUCTION

Tungsten trioxide is one of the most intensively studied electrochromic materials (see, e.g., the review by Granqvist[1]). This class of materials is of great technological importance for the development of tunable reflection coatings, which could find applications in such various devices as television screens and windows.

In spite of substantial research effort, understanding of the electrochromic mechanism is still not complete. Upon application of an electric field over the electrochromic device, electrons and charge-compensating monovalent ions (e.g., H^+, Li^+, Na^+) diffuse into the material and give rise to a modification of its optical properties. In thin films of disordered WO_3, this intercalation results in a strong, broad absorption band at ≈ 1.2 eV. In crystalline WO_3, the electrochromism is less effective (see, e.g., Refs. 1 and 2). In this paper, we restrict ourselves to the study of highly disordered, i.e., amorphous WO_3 (a-WO_3) as a model for thin-film tungsten trioxide.

Direct d to d transitions being very weak in general, it is not a surprise that explanations of the occurrence of this absorption band in a-WO_3 in terms of direct transitions between the tungsten states fail. Instead, a more sophisticated mechanism is sought. By far the most promising explanation was put forward by Faughnan, Crandall, and Heyman,[3] who proposed a model based on intervalence charge transfer (IVCT). Later, this model was refined by Gabrusenoks *et al.*[4] using the theory developed by Bryskin.[5] The archetypical compound exhibiting this coloration mechanism is Prussian blue. The underlying theoretical ideas are described in Ref. 6. In short, they amount to the following: Assuming a complete charge transfer of the tungsten valence electrons to oxygen states to start with (i.e., an ionic octet compound), the excess electrons localize at the tungsten sites. Thus W^{5+} species are created in a background of W^{6+} sites. The absorption of light then arises from a (phonon-mediated) excitation of an electron in one such W^{5+} site to a neighboring W^{6+} site:

$$W_a^{5+} + W_b^{6+} \xrightarrow{h\nu} W_a^{6+} + W_b^{5+} .$$

The ''hopping'' electron carries along a distortion of the ''lattice,'' so that the process can also be described in the language of polarons. Indeed, Schirmer, Wittwer, Baur, and Brandt (Ref. 7) have proposed a model involving ''small polaron absorption'' [and also the paper by Bryskin (Ref. 5) employs that language]. Moreover, the IVCT intensity should be significantly enhanced by vibrational excitations of the ''lattice'' distortions (related to the localized excess electron).

The above explanations provide a simple model that can describe the shape of the experimental absorption curve satisfactorily. It is supported by the occurrence of a very weak electron-spin-resonance signal (first reported by Deb, Ref. 8) in colored a-WO_3 films, which is interpreted to originate from the unpaired electron on the W^{5+}. However, these explanations do not provide a clear picture of the microscopic structure of a-WO_3, i.e., what the surroundings of the optical center look like, how these are different from the crystalline phase, and how (de)localized are the initial and final states of the optical transition. Moreover, they provide an incomplete description: for instance, oxygen-deficient films can remain colorless even though an appreciable fraction of W^{5+} should have formed. This was pointed out recently by Zhang *et al.*,[9,10] who proposed to solve this problem by assuming the existence of a W^{4+} species.

In this paper, a qualitative picture of the microscopic structure and electronic structure of amorphous WO_3 is obtained by means of first-principles density-functional calculations, using an approach similar to the Car-Parrinello method.[11] Small samples were generated that should exhibit the main features of the amorphous phase, and their electronic structure is discussed. Further, it is attempted to assess which ''defect'' structures can give rise to IVCT-like excitations and which do not.

Section II deals with the computational details. Results and discussion of the (electronic) structure of the computer-generated samples are presented in Sec. III. In Sec. IV, experimentally observed W^{5+} species in bulk systems are compared to those found in computer-generated a-WO_3. Conclusions are summarized in Sec. V.

 ©1999 The American Physical Society

II. COMPUTATIONAL DETAILS

The calculations have been performed using the *ab initio* total-energy and molecular-dynamics program VASP (Vienna *Ab Initio* Simulation Program) developed at the Institut für Theoretische Physik of the Technische Universität Wien.[12–14]

Electron-ion interactions were described using Vanderbilt ultrasoft pseudopotentials (USPP) (Ref. 15) with a frozen $[\mathrm{Xe}]4f^{14}$ and $1s^2$ core for W and O, respectively, and using a norm-conserving pseudopotential with [Ne] core for Na. The pseudopotentials were supplied by the Institut für Theoretische Physik.[16] Nonlinear core corrections were applied for W and Na.[17] For efficiency, in calculations on larger cells, the real-space projection scheme by King-Smith *et al.* for the nonlocal part of the pseudopotentials was used.[18]

Most calculations were done in the local-density approximation (LDA) using the parametrization by Perdew and Zunger (Ref. 19) of the Ceperley and Alder functional.[20] For the few calculations done in the generalized gradient approximation (GGA), the gradient corrections following Perdew *et al.*[21] (PW 91) were adopted. The preference for LDA over GGA calculations was motivated by the better agreement with the experimental structural parameters obtained with the former for crystalline WO_3 (c-WO_3).[22] Further details concerning the electronic-structure part can be found in Ref. 22.

Amorphous samples were created by quenching from a hot liquid. A few calculations were done in the GGA (results nor reported), and such a structure (already disordered) was taken as input for the LDA calculations, where the size of the box was rescaled to the LDA volume. This sample was rapidly heated to $\sim$5000 K, i.e., far above the experimental melting point at ambient conditions (1745 K, Ref. 23). Then the system was allowed to evolve, running a microcanonical molecular dynamics (MD), until the atoms had on average moved at least one nearest-neighbor distance. This was done to make sure that the crystalline ordering was really destroyed. After the ''equilibration,'' MD was continued and every 70 steps (0.14 ps) a configuration was selected. These configurations were quenched (with a CG minimization). This way, a small ensemble of 10 amorphous configurations was obtained. Due to the disparity between the W and the O mass, the W atoms are expected to move slower. This inefficiency was circumvented by running with smaller W mass (40 and, occasionally, 16 amu).

The quench was carried out very abruptly with a CG minimization. More careful minimizations are possible, e.g., by slowly cooling the system. However, since our concern was not with great detail and since this would have been computationally much more demanding, we opted for this rather crude method. This amorphization procedure is a tool to approximate a structure that is created experimentally under conditions far from thermodynamic equilibrium (e.g., growth by sputtering), where kinetic inhibitions should play a major role in determining the local structure.

Calculations were carried out in a cubic supercell [7.48^3 Å^3, LDA volume] with periodic boundary conditions applied and containing eight formula units. One check on the size effects was done with a larger cell that contained 27 formula units [11.22^3 Å^3, same LDA density]. This configuration was generated in a way similar to the procedure outlined above for the eight formula units cell. No experimental data were available for the density of a-WO_3, so the calculated equilibrium volume for the monoclinic crystal was taken.[22] In a recent study, density estimates for sputtered films were given.[24] However, as these films probably contained water, the estimates can only serve as an upper bound ($\sim$6% larger ''lattice'' dimensions than monoclinic WO_3). Because c-WO_3 can be compressed very easily (due to rotation of structural units, see, e.g., Ref. 22), and since presumably the same holds for a-WO_3, we expect large fluctuations in the local density anyway. In our calculations we do not find an unacceptably high pressure.

TABLE I. Several details of the ten amorphous WO_3 samples. Total energies are per WO_3.

	$E(\frac{1}{4},\frac{1}{4},\frac{1}{4})$ (eV)	$E(3\times3\times3)$ (eV)	Gap (eV)
	monoclinic crystal		
	0		1.1
	simple cubic crystal		
	0.01	0.04	1.14
	amorphous WO_3		
1	0.90	0.91	2.0
2	0.95	0.95	1.8
3	1.00	0.99	1.9
4	1.19	1.22	0.1
5	0.86	0.86	2.3
6	1.04	1.03	2.2
7	0.87	0.88	1.7
8	1.09	1.11	2.1
9	0.88	0.88	1.9
10	0.96	0.97	1.9

During the MD and quench, the Brillouin zone (BZ) was sampled with just one **k** point [$(\frac{1}{4},\frac{1}{4},\frac{1}{4})$, for reasons of efficiency in the large cell Γ was used for the MD and in a prerelaxation]. The electronic density of states of a quenched sample was calculated with a $3\times3\times3$ mesh (centered on Γ) without additional optimization.[25,26] This provides an *a posteriori* confirmation that one **k** point was sufficient for the structural optimization (see Table I).

To see whether states where sufficiently localized to accommodate unpaired electrons, i.e., whether magnetic solutions are stable, local-spin-density calculations were carried out for a few promising candidate structures. Some of the configurations with a very large density of states at the Fermi level were selected. The GGA was employed, as the LDA generally underestimates the stability of magnetic solutions. The geometry was not relaxed and stabilizing energies were calculated as the energy difference with non-spin-polarized GGA calculations.

III. RESULTS AND DISCUSSION

This section is structured around the 10 amorphous configurations that were obtained for the cell with eight formula units (within the LDA). First, the 10 stoichiometric configurations (as obtained by quench during the MD) are dis-

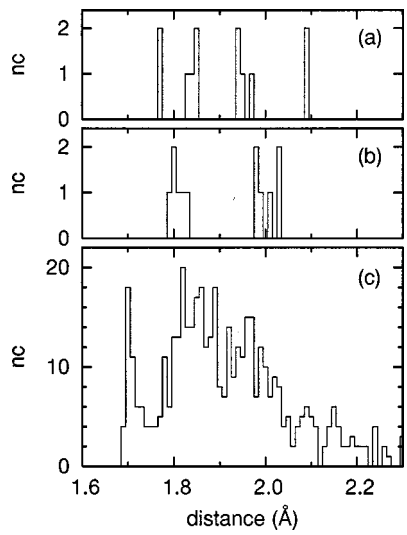

FIG. 1. The relative number (nc) of occurrences of nearest-neighbor W-O distances, for (a) the monoclinic crystal, (b) the artificial crystal in the cubic box, and (c) the 10 amorphous configurations.

cussed and compared to the single stoichiometric a-WO_3 configuration with 27 formula units.

Next, samples with a filling of some of the conduction-band states are considered. This can be attained by either a deficiency of oxygen (incomplete charge transfer from tungsten to oxygen atoms) or by intercalation with alkali-metal atoms (that donate their valence electrons) or both. Experimentally it is known that both situations result in a different optical behavior. These situations are mimiced in an attempt to identify the crucial difference in the donation of electrons into the conduction band.

All the ''doped'' samples are derived from the 10 stoichiometric configurations of eight formula units. Arbitrarily one or two oxygen atoms were removed and the structure relaxed into the nearest local minimum (using a CG minimization). The alternative was modeled by adding one or two Na atoms. These were inserted so that their nearest neighbors were at maximal distance and followed by a relaxation. After one Na was added and the structure relaxed, the same procedure was repeated adding a second Na. Also, configurations both short of oxygen and with Na added were made, starting from the oxygen-deficient samples.

A. Stoichiometric a-WO_3

1. Structure: Atomic arrangement

Figure 1(c) depicts the distribution of nearest-neighbor W-O distances for the 10 samples. This distribution is also shown for the monoclinic crystal [Fig. 1(a), theoretical structure] and for a hypothetical crystal in a cubic box [Fig. 1(b), at the same volume]. The hypothetical crystal is used to discriminate between the effect of amorphization (in the cube) and of the deformation of the crystal (monoclinic → cubic box). The proper monoclinic cell is not very different from the cube, so the change of shape should not have dramatic effects on its properties. Indeed the effect, after optimization of the atomic positions, is rather small.

The monoclinic structure consists of corner-sharing distorted octahedra. Oxygen atoms are at the corners of an octahedron and a tungsten atom occupies a position slightly off center. This gives rise to a structure with infinite chains of alternatingly long and short W-O bonds running in all three crystallographic directions. This feature is clearly visible in the bond-length distribution of Fig. 1(a). It also reflects that the long-short splitting is not the same for each direction. In the artificial cube [Fig. 1(b)], the splitting of W-O bonds into relatively short (~1.8 Å) and long (~2.0 Å) bonds remains, but any additional structure in the bond-length distribution disappears.

TABLE II. Distribution of the number of oxygen neighbors (N_O) of tungsten atoms. A cutoff $r_c = 2.3$ Å was used.

N_O	Count	
	$8\times WO_3$	$27\times WO_3$
1	0	0
2	0	0
3	0	0
4	5	1
5	26	5
6	47	15
7	1	5
8	1	1
9	0	0
10	0	0

In the amorphous samples, the long-short splitting cannot be easily discerned: The very broad peak in the bond-length distribution shows that all bonds from ~1.8 Å to more than ~2.0 Å are likely to occur. An important feature is the narrow peak near ~1.7 Å. This peak originates from singly coordinated oxygen atoms, i.e., oxygens that are bound to only one tungsten atom. Such bonds do not occur in the crystal. Only about half of the tungsten atoms have a bond with such an oxygen atom. That two such oxygen atoms are bound to one tungsten happens only rarely.

The coordination of tungsten by oxygen (Table II) provides another indication of how far the system has moved from crystallinity. In the crystalline samples, only sixfold-coordinated tungsten occurs. In the amorphous samples the sixfold coordination is still dominant, but also an appreciable amount of fivefold- and fourfold-coordinated tungsten is found. The occurrence of singly coordinated oxygen atoms can account for most of this coordination ''deficiency:'' integrating the table, one finds on average a shortage of approximately four O-W bonds per amorphous sample, which matches almost all of the area under the first (sharp) peak in Fig. 1(c). The small difference has to be accounted for by rare defects such as triple-coordinated oxygens.

Most tungsten atoms still being (close to) sixfold coordinated by oxygen, one may wonder how much of the octahedral character of the first coordination shell has remained. A good indication comes from the bond angles (θ). Figure 2 shows their distribution for the crystal and the amorphous samples as a function of $\cos(\theta)$.[27] The perfect octahedral coordination is characterized by two peaks in the O-W-O angle distribution: one at 0 ($\theta = 90°$) and one at -1 ($\theta = 180°$). Moreover, these occur in the ratio 4 (90°) to 1 (180°). This applies to the crystals [Figs. 2(a) and 2(b)], although—due to the distortions—these features are smeared

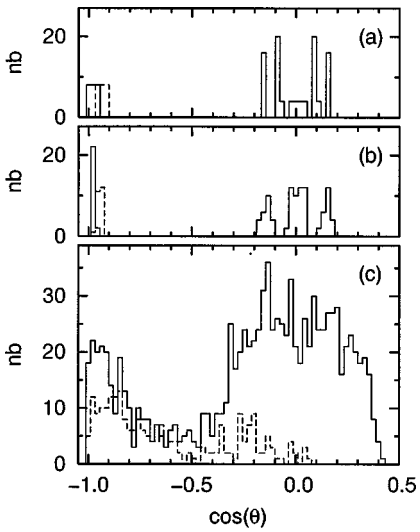

FIG. 2. Bond-angle distributions (nb). O-W-O bonds: solid line, W-O-W bonds: dashed line. A cutoff distance $r_c = 2.3$ Å was used. $r_c = 2.8$ Å gives almost identical results. (a) monoclinic crystal, (b) artificial crystal in the cubic box, and (c) the 10 amorphous configurations.

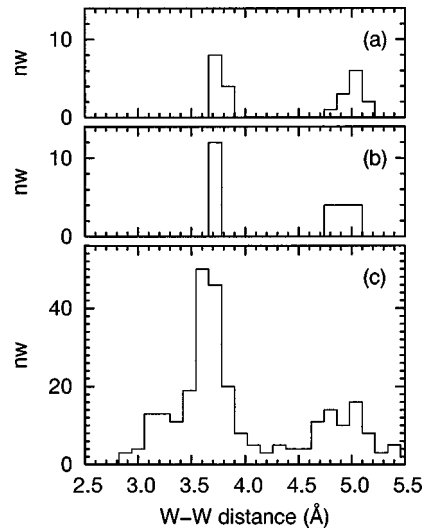

FIG. 3. W-W distances distribution (nw) using the minimum image convention. See Fig. 1.

out to some extent. In the amorphous samples the peak at 0 is still very prominent. It has broadened, but not shifted. Given that the average number of oxygen neighbors is still close to six, in this way the (negatively charged) oxygens avoid closely approaching one another. The peak near -1 is also clearly resolved, and constitutes a marked remnant of the octahedral ordering. However, both peaks are not separated anymore, as any angle in the range 90° to 180° is possible. Superimposing an (artificial) picture, in which all W are still maximally octahedrally coordinated, and imposing the 4:1 ratio to separate bond angles in those derived from the 90° and 180° peaks, results in $\cos(\theta) = -0.65$, i.e., $\theta = 130°$. This means that octahedra, as far as they can still be discerned, are highly distorted.

The W-O-W angles (also in Fig. 2) give information about the ''interoctahedral'' correlations. In the crystals, the peak near -1 (180°) is indicative of the chainlike arrangement of the octahedra. In the amorphous samples, this feature has almost completely vanished, all angles from $\sim 90°$ and larger being possible. The occurrence of such small W-O-W angles suggests a kind of bridging geometry of the oxygen linking together two tungsten atoms (see below).

The distribution of W-W distances is plotted in Fig. 3.[28] Again, the distance distribution is smeared out a lot in the amorphous samples. Note that there is a tail extending to rather small W-W distances (ranging to ~ 3.0 Å). Short distances play a role in the in-gap states in the doped samples discussed in Sec. III B.

In order to asses the importance of possible size effects, we also generated one configuration with 27 (instead of 8) formula units in the periodic cube. The structural characteristics are compiled in Fig. 4. As the data derive from only one sample, the curves are a bit noisier than for the smaller cell averages. Within the noise, the W-O distance (Fig. 1), angle (Fig. 2), and W-W distance distributions (Fig. 3) of the small cell are similar to those of the large cell (Fig. 4). Also here all W-O bonds contributing to the isolated peak at 1.7 Å in the W-O distance distribution pertain to singly coordinated oxygen atoms. A minor, but striking, difference is the extra peak at $\cos(\theta) = 0.7$ that indicates a very small O-W-O angle ($\theta \sim 45°$). This small angle derives from one O-O pair (of two) that is bound with both oxygens to a W atom. These two O-O pairs have 1.43 and 1.47 Å interatomic distances, i.e., just slightly smaller than typical peroxide O-O distances (1.5 Å), but still larger than typical superoxide O-O distances (1.3 Å).[29,30] Only one such O-O pair occurs in the 10 small samples. It is probably an artifact of the rather crude amorphization procedure.[31]

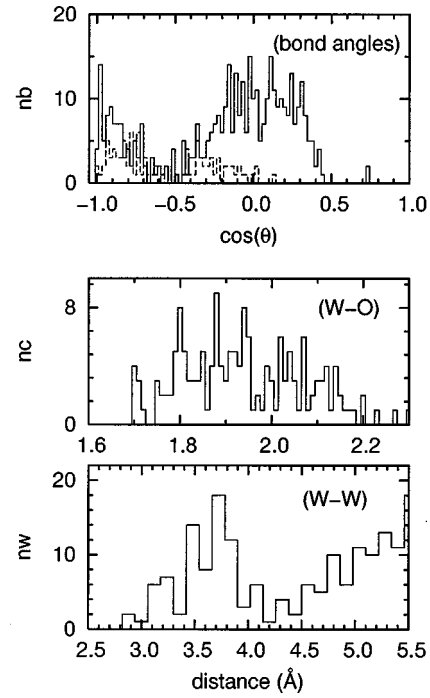

FIG. 4. Amorphous configuration with 27 formula units. Top panel: O-W-O and W-O-W angle distributions, full and dashed curves, respectively. A cutoff of 2.3 Å was used to define a W-O bond. Middle panel: W-O distance distribution. Lower panel: W-W distance distribution.

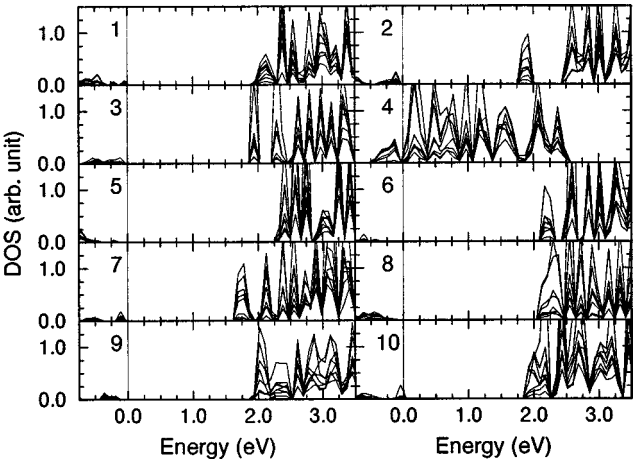

FIG. 5. Partial tungsten densities of states for the 10 stoichiometric configurations. The zero of energy is at the Fermi level or (in case of a finite gap) at the top of the valence-band region.

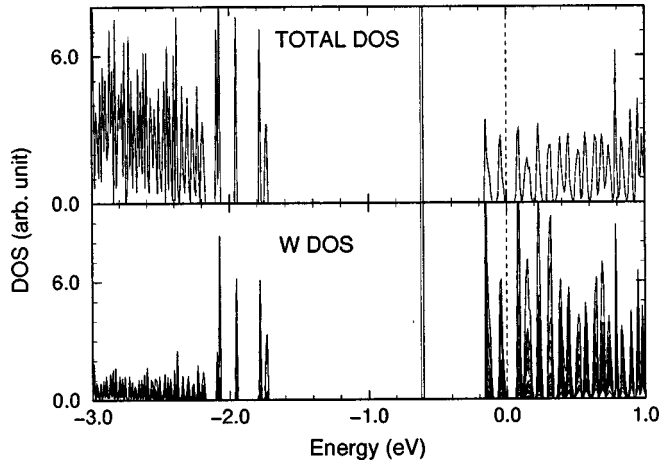

FIG. 6. Density of states for the amorphous configuration with 27 formula units. Upper panel: total DOS, lower panel: partial W densities of states.

2. Electronic structure, band gap

The electronic properties also differ from those of c-WO_3. Table I lists the band gaps of the 10 amorphous samples and the monoclinic and artificial simple cubic crystals. The partial tungsten densities of states are depicted in Fig. 5. Although the size of the gap varies appreciably between the amorphous configurations, it is significantly higher than in the crystals. In parallel with this gap widening, a narrowing of the bands occurs. In fact, in a-WO_3, contrary to c-WO_3, there are no infinite one-dimensional (1D) -O-W-O-W- chains that can give rise to a sizable dispersion. The monoclinic crystal (Ref. 32, gap at Γ) exhibits such 1D chains (although a bit distorted) and the near-gap conduction bands are far more dispersive (of the order of ~ 1 eV). So the band-gap widening in a-WO_3 can be understood as the absence of the band-broadening mechanism effective in c-WO_3. This explanation is supported by the rather open structure of the material: If a 1D chain of interactions is disrupted, there are not many possibilities to repair the disruption. Such a situation cannot arise in a close-packed material, where there are always atoms present to mediate the interaction.

Configuration 4 drops out from the picture outlined above, having a gap of merely ~ 0.1 eV. Such a seemingly ''extreme narrowing'' also occurs for the single configuration with 27 formula units. Inspecting the (partial) densities of states (Figs. 5 and 6), it emerges that what happens is not a suppression of the band-gap widening, but a filling of the lower part of the conduction band. This is a consequence of the (probably artificial) formation of the O-O bonds mentioned above (also configuration 4 and the large sample), and hence probably an artifact. The formation of a bond between the oxygen atoms frustrates a complete charge transfer and expels two electrons into the tungsten-derived states (i.e., conduction bands). In the large cell, these O-O bonds are also responsible for the in-gap states: all the bands with unusually large tungsten contributions in the valence-band region have significant contributions of one of these O pairs, and the state near -0.55 eV is localized on one O-O pair.

Another marked feature is the absence of states in the gap (except for those caused by the artificial O-O bonds), although bonds have been broken. In part, this is just another aspect of the mechanism outlined in the previous paragraphs: In any material of the stoichiometry WO_3 one naively expects a gap of ionic character, irrespective of the number of bonds $[W^{6+}(O^{2-})_3]$. The absence of infinite ''1D'' -O-W-O-W- chains [by disorder, and through a breaking of bonds by a reduced number of interactions between $W^{6+}(O^{2-})_3$ units] results in frustration of band broadening, i.e., band-gap widening. However, this naive picture disregards the effect of the local ''crystal'' field. If large variations occur, they may well push several levels into the gap. The absence of in-gap states shows that for stoichiometric a-WO_3 this mechanism is only of minor importance. This is a nontrivial result. For example, for NaCl, vacancy-interstitial pairs (i.e., a stoichiometric defect structure) can already give rise to in-gap states.

Band-gap widening in disordered films has also been observed experimentally, and can be as much as 0.6 eV (See Ref. 1 for an overview and discussion). Possible reasons put forward in the literature are structural transformations and quantum confinement. In the context of the present study, it is not possible to address the first. However, this mechanism is consistent with our calculations on the WO_3 crystals, where for the monoclinic low-temperature phase a gap about 0.2 eV higher than for the room-temperature monoclinic phase was found.[22] Indeed, the experimental argument for this possible reason is based on a gap increase of 0.2–0.3 eV on cooling to $-50\,°C$, as reported in Refs. 33–35. The other mechanism (quantum confinement) is somewhat similar to the mechanism outlined in the previous paragraphs. Quantum confinement arises because the length over which the electrons are free to move is limited. This is not exactly the case in our samples, where only the band broadening is frustrated because the crystalline order has broken down. But, effectively, this means that the length over which electrons are free to interact has considerably decreased.

3. Electronic structure, conduction-band states

Paralleling the conduction-band narrowing, there is a clear tendency for the conduction-band states to localize on a few tungsten atoms. This is evident from the partial W den-

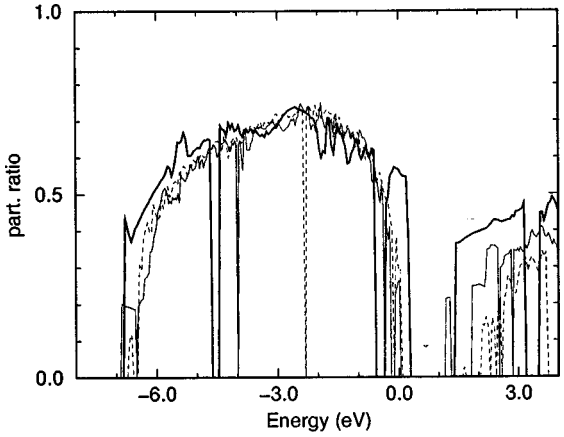

FIG. 7. Participation ratios. Cutoff radii for the tungsten and oxygen site projection were 2.086 and 1.042 Å, respectively (for the DOS plots, a radius of 0.759 Å was used; trends are not affected by this difference). The thick line pertains to the crystal as confined to a cube, the full thin line to an oxygen-deficient amorphous structure in a small box, and the dashed line to the large amorphous cell. The energy axes are shifted so as to have the valence bands aligned.

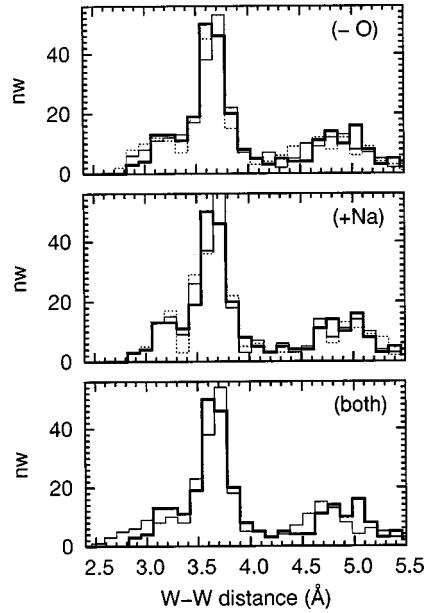

FIG. 8. W-W distances distribution (nw) using the minimum image convention. The thick line is the distribution for the stoichiometric amorphous sample as in Fig. 3. Thin and dashed lines belong to the ''doped'' samples. For the upper two panels they denote one oxygen (Na) and two oxygens (Na) removed (added), respectively.

sities of states (Figs. 5 and 6): The narrow bands (peaks) that can accommodate two electrons have very different amplitude on different tungsten atoms. In the large box (27 formula units), the conduction bands have become narrower and closer spaced as compared to the small samples. Therefore, the larger box does a better job in estimating the dispersion and thus allows for a better view on the localization region of the states. These are not confined to just one or two atoms in general, but can encompass many atoms and can have significant amplitude on even half the tungstens in the box (although a few dominate). Extrapolating to a very large box, this leads to a continuous distribution of states on the energy axis, but—due to their localized character—only a finite number will have an amplitude in a certain spatial region of the solid, where states will be separated by small, but finite, energy intervals.

The above-mentioned tendency towards localization of the conduction-band states can be put on a more quantitative basis by means of the participation ratio p_i.[36] It is defined as

$$p_i = \frac{\left(\sum_{j,l} |e_{i,l}(\mathbf{R}_j)|^2\right)^2}{N\sum_{j,l} |e_{i,l}(\mathbf{R}_j)|^4},$$

where $e_{i,l}(\mathbf{R}_j)$ denotes the eigenstate projection of band i for the atom at site R_j and angular momentum channel l. In monatomic systems, it provides an easy means to estimate the degree of localization of a state (''band''): For delocalized states it approaches 1 and for a state localized on one site only it is $\sim 1/N$ (where N denotes the number of atoms in the cell). For a diatomic system the interpretation is a bit tricky, since the relative size of the $\{e_{i,l}(\mathbf{R}_j)\}$ depends on the ratio of the radii used in calculating the site projection. In spite of this trouble, it remains a useful tool for comparing the localization behavior *as a function of box size.*

In Fig. 7, we show the average participation ratio, i.e., the sum of p_i per unit energy normalized by the total density of states. Therefore, the plot does not contain information on the spread of p_i at fixed energy. The crystalline solid (in the cube), a typical amorphous configuration from the small box,[37] and the amorphous configuration in the large box are compared. For the bulk of the oxygen $2p$-derived valence band, all samples behave very similarly: the curves coincide and attain a peak value of ~ 0.75. This is the limiting maximum value for states that are fully delocalized on three quarters of the atomic sites (i.e., the oxygen sites), so we may conclude that, even in the amorphous samples, the valence-band states remain quite delocalized (''dispersive''). In accordance with expectation, at the edges of the valence-band region, states tend to localize. For the conduction bands, the story is quite different. In going from the crystal to the small amorphous sample, there already is a significant drop, i.e., a tendency towards localization. Going from the small to the large box there is again a drop, demonstrating that the conduction-band states really are localized. The drop does not scale as $1/N$, showing that the states were not yet decoupled from their periodic images in the small amorphous sample.

B. Oxygen-deficient a-WO_3

Removal of an oxygen atom constitutes considerable damage, and thus offers the possibility of significant relaxation. The consequences are most significant for the W-W distances (Fig. 8). Although the general picture does not change much, a significant increase in the number of very short W-W distances is evident. That is, oxygen shortage enables the W atoms to ''see'' the others more easily (which opens up the possibility of additional interactions).

The O-W nearest-neighbor distances (nc) are not much affected (Fig. 9). The number of short bonds (at ~ 1.7 Å)

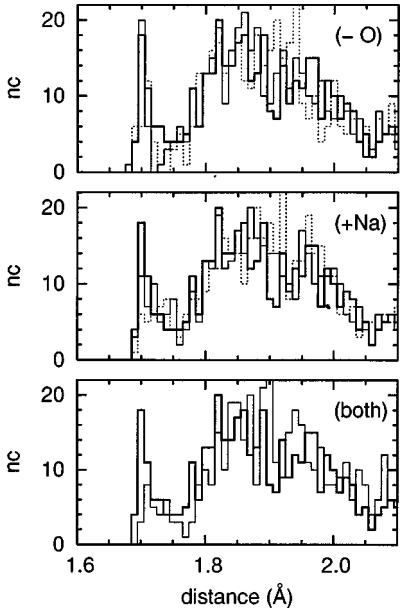

FIG. 9. O-W distances distribution (nc), see Figs. 1 and 8.

remains almost the same (these bonds seem to be more clearly separated from the others by a deeper minimum).

Figures 10 and 11 depict the partial tungsten densities of states for the 10 configurations with one and two oxygen atoms removed, respectively. The tendency of the conduction bands to localize is again evident. New features have developed in the gap region. Oxygen removal can result in filled, deep in-gap states that are clearly separated from the conduction bands. This is most pronounced in the configurations 5, 6, 9, and 10 with two oxygens removed.

The occurrence of these deep in-gap states is related to the short W-W distances: These states have a relatively large DOS on just two tungsten atoms and these pair with a relatively short interatomic distance. The respective interatomic distances are 2.80, 2.96, 2.88, and 2.72 Å for configurations 5, 6, 9, and 10. Thus the relaxations induced by oxygen shortage, can result in in-gap states that are well localized on tungsten pairs. All these tungsten pairs are characterized by a relatively short interatomic distance. In Fig. 12 we show a few typical configurations [(a) and (b) pertain to configurations 9 and 10, respectively]. For configuration 9, the in-gap state is localized on W2-W3. This pair is bridged by just one oxygen atom. The pair W1-W2 is not associated with an

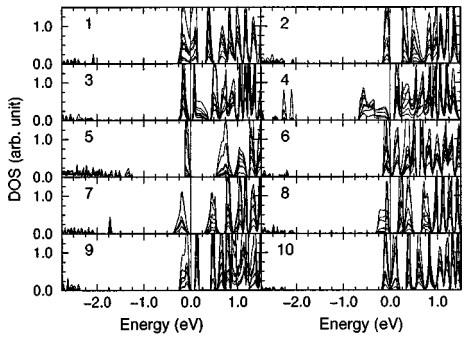

FIG. 10. Partial tungsten densities of states for the 10 configurations with one oxygen atom removed.

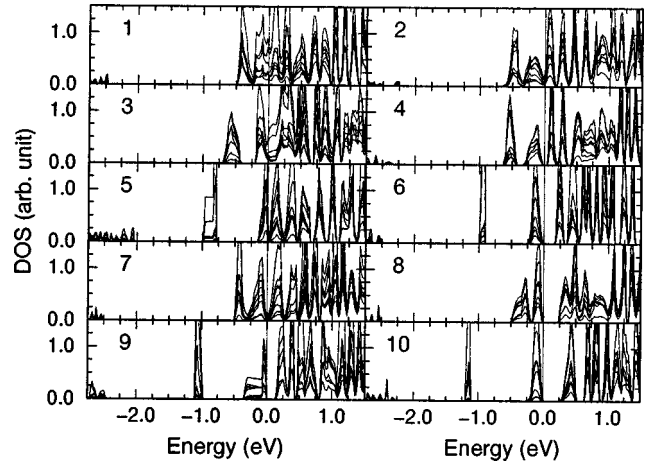

FIG. 11. Partial tungsten densities of states for the 10 configurations with two oxygen atoms removed.

in-gap state. It is bridged by at least two oxygen atoms. In configuration 10, the in-gap state is localized on the pair W1-W2. This pair seems to be bridged by one oxygen, however as one W-O length is rather long, it is better to consider it not bridged at all. The pair W2-W3 is not associated with an in-gap state, and is bridged by two oxygen atoms. In general, a close W-W approach is not a sufficient condition

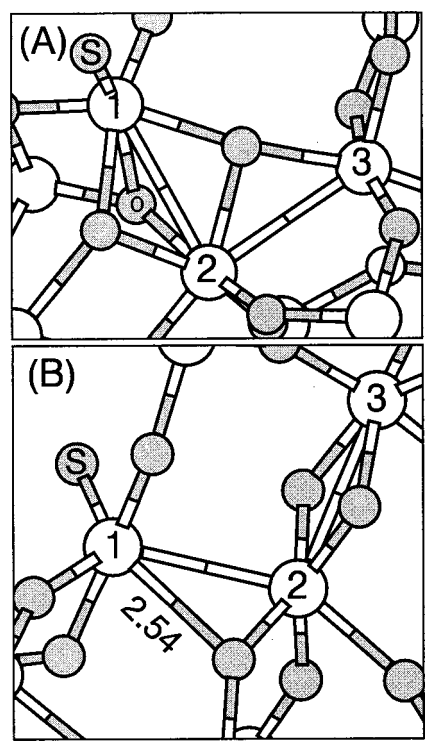

FIG. 12. Two oxygen-deficient configurations (W_8O_{22}) with tungsten pairs. (a) Configuration 9, (b) configuration 10. Tungstens are represented by large white spheres, oxygens by small gray spheres. Three selected (numbered) W atoms are shown with their immediate surroundings. Singly coordinated oxygens are denoted by S. The other W-O distances are in the range 1.9–2.1 Å, except for $d_{1o}=2.36$ Å in (a) and the 1.54 Å distance in (b). Interatomic distances: (a) $d_{1s}=1.70$ Å, $d_{12}=2.94$ Å, $d_{23}=2.88$ Å; (b) $d_{1s}=1.72$ Å, $d_{12}=2.72$ Å, $d_{23}=2.91$ Å.

TABLE III. Magnetic moments (μ_B) and energies (ΔE). N_{con} denotes the number of the amorphous configuration and the next two columns the number of removed oxygen and added sodium atoms. Magnetic moments are listed only for those configurations where a spin-polarized solution was found. ΔE is the energy reduction compared to the non-spin-polarized solution.

N_{con}			μ_B/cell	ΔE (meV)
1	−2O	+2Na		
1	−2O			
1	−O			
2		+Na	1.0	1
3	−2O	+2Na	0.6	−4
5	−O	+Na	0.75	−8
5	−2O	+2Na		
8		+2Na	0.85	31
8		+2Na	2.0	49
8		+Na	1.0	8

for the occurrence of in-gap states. Only in those instances where the W-W ''bond'' is not bridged by two oxygens (reminiscent of an edge sharing between tungsten-containing oxygen octahedra) are in-gap states found to occur. In Sec. III D this picture will be qualified.

Note that those excess electrons not accommodated by the in-gap states just fill the conduction bands. This occurs (in general) in a band-by-band fashion where each pair of electrons fills one band. Therefore (even number of electrons), the Fermi level ends up in a deep minimum. Consistently, no stable magnetic solutions are found for the oxygen-deficient configurations in Table III.

C. Stoichiometric *a*-WO_3 with Na added

Contrary to oxygen removal, Na addition does not induce considerable structural rearrangements. The distribution of W-W distances hardly changes (Fig. 8) and the network of O-W bonds is left almost unaffected. In spite of this, a suppression of the number of short O-W distances is evident (Fig. 9). In part, this can probably be put down to a steric effect: The Na atoms take up additional space and thus force singly coordinated oxygen atoms closer to other tungsten atoms. The result could be the formation of an additional O-W bond. Thus the oxygen atom is not singly coordinated anymore and its old O-W bond distance has moved away from the peak in *nc* at 1.7 Å. Indeed, in both configuration 1 and (the slightly pathological) configuration 4, two singly coordinated oxygen atoms have become doubly coordinated after insertion of two Na atoms. However, this is not sufficient to explain the whole effect. For the rest, the shift of the peak results from just an elongation of all the W-O bonds (on average). It is unlikely that this effect is related to localization of the excess electrons (i.e., those donated by Na) on tungsten atoms, since then a similar effect should be expected for the oxygen-deficient samples. The most plausible mechanism remaining is related to the presence of the positive ''ion'' Na^+. Its nearest neighbors are (negative) oxygens. The (positive) tungstens are not found closer than in the second nearest-neighbor shell. In this way, a Na^+ species can stretch the O-W bonds without affecting the network

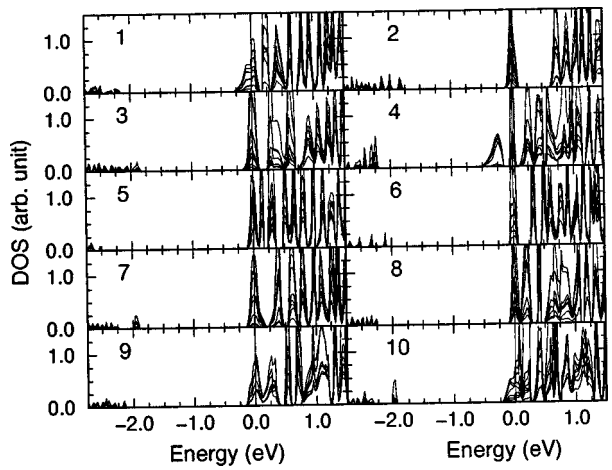

FIG. 13. Partial tungsten densities of states for the 10 configurations with one Na atom added.

formed by these bonds. Unfortunately, it is difficult to unambiguously identify this mechanism since a test would necessitate removal of the Na^+ charge without removing the atom itself (steric effects) and its donated valence electron.

Figures 13 and 14 depict the tungsten densities of states for the 10 configurations (one and two Na's added, respectively). Again, the tendency towards localization and the narrow bands in the conduction-band region are evident. Contrary to the case of oxygen removal, no in-gap states result.[38] Excess electrons end up in the conduction-band states, giving rise to half-filled bands for one Na^+ and one electron added. These bands have an appreciable DOS at the Fermi level and thus an exchange splitting could possibly stabilize a magnetic solution. The stability of a magnetic solution differs from case to case (Table III). For example, in sample number 2, doping with one Na gives a half-filled, rather flat and isolated band, so a magnetic solution should be possible. Indeed we find one, but it is degenerate in energy with the nonmagnetic solution. The width of the band is not really zero, reflecting some interaction with neighboring supercells, which favors some delocalization and a nonmagnetic flat metallic band. In sample 8, the filled conduction band(s) seem(s) a bit flatter, and a magnetic solution is not only

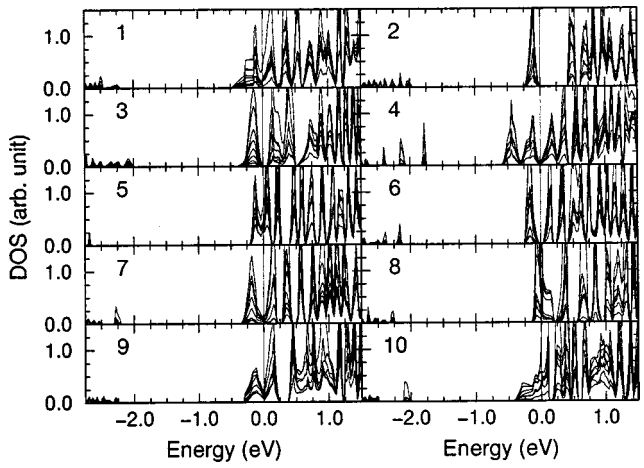

FIG. 14. Partial tungsten densities of states for the 10 configurations with two Na atoms added.

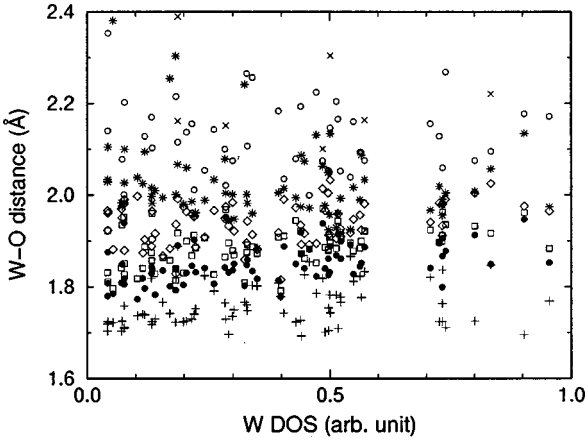

FIG. 15. W-O distance as a function of W excess charge, for the stoichiometric configurations with two Na atoms added. The excess charge was obtained by integrating the local W DOS from -0.5 eV to the Fermi level. The excess charge depends on the projection radius used to calculate the site-projected DOS, and its absolute value is not very meaningful. It was rescaled to fit the interval 0-1. Symbols used to denote the O-W bonds, in order of increasing length, are +, ●, □, ◇, *, ○, ×.

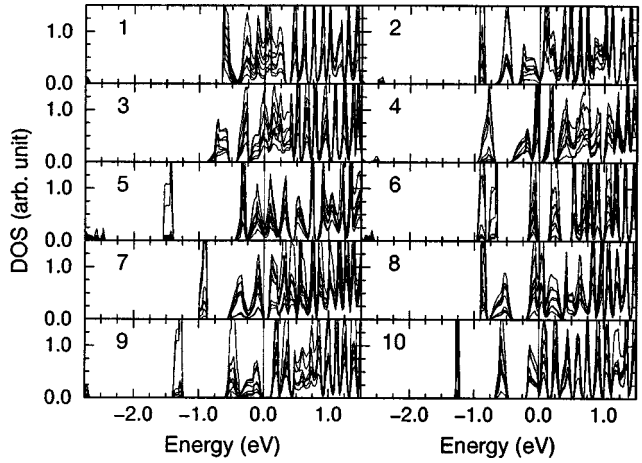

FIG. 16. Partial tungsten densities of states for the 10 configurations with two oxygen atoms removed and two sodium atoms added.

possible, but also energetically favored (even with two Na's added). Sample 5 does not look favorable at all, at least with two sodiums added and also two oxygens removed, and indeed no magnetic solution was found possible. Sample 5 with one Na added and one O removed looks rather similar to sample 1 with one Na removed. Nevertheless, a magnetic solution is possible, but it is not energetically favored. The instability of the magnetic solutions in some of these cases can well be an artifact of the small size of the supercell (too dispersive bands reduce the density of states at the Fermi level).

A clear correlation between the local surroundings of the tungsten atoms and their affinity with the excess electrons provided by the Na atoms could not be discerned. This is demonstrated, for example, by Fig. 15, which refers to the stoichiometric configurations with two sodium atoms added. It shows the length of the bond to the nearest, next-nearest, etc. oxygen atom as a function of the excess charge localized on the tungsten atom for all tungstens and all ten configurations. The excess charge was obtained by integration of the local W DOS from inside the gap to the Fermi energy. Any clear structure is absent in the figure. This implies that the excess electrons do not tend to localize preferentially near short W-O bonds.

D. Oxygen-deficient a-WO_3 with Na added

These configurations were made by adding Na atom(s) to the oxygen-deficient samples (W_8O_{22}).

For the W-O distance distribution nc (Fig. 9), a similar change of oxygen coordination occurs as when Na's are added to the stoichiometric structures, i.e., nc is considerably suppressed at short distances (even at ~ 1.8 Å). This is consistent with, and thus supports, the explanation from the preceding paragraph: only when Na^+ is present can it pull at the negative oxygens and push on the positive tungstens, and therefore give rise to a bond elongation.

Concerning the W-W distances, the effect of Na addition is somewhat different for the oxygen-deficient than for the stoichiometric samples (Fig. 3). Na addition helps to increase the number of short W-W distances that were already triggered by oxygen removal. Apparently, the small disruption of adding a Na atom helps to find a new local minimum more favorable for W-W bond formation.

The electronic spectrum is depicted in Fig. 16. Again, a clear tendency towards localization of the conduction bands is evident as well as a significant number of in-gap states. As more short W-W distances do occur, we expect also more in-gap states.

All in-gap states that were already present in the structures with only oxygen removed are still present. However, more have also appeared. For example, in configuration 2, a tungsten pair (2.64 Å) gives rise to a localized state at -0.9 eV (the top of the peak is far outside the plot). Interestingly this tungsten pair is bridged by two oxygens. This suggests that somehow the disadvantage of having two bridging oxygens is offset by the very small interatomic distance of 2.64 Å. Also, one can argue that the state does not lie very deep. A similar borderline case occurs in configuration 4. Here two tungsten pairs (2.69 and 2.85 Å) are jointed by a common W atom and both pairs are bridged by two oxygens. The resulting peak (at -0.9 eV) is rather broad and not so far from the conduction bands. Configuration 5 has remained as it was before: one tungsten pair (2.77 Å) with only one ''bridging'' oxygen (with a long W-O distance of 2.38 Å). Indeed, a very deep in-gap state results. Configuration 6 warrants special attention. Here there is a two-peak structure (-0.8 eV) involving two tungsten pairs (again with a common W). The pair with 2.99 Å distance was already present in the oxygen-deficient structure before Na was added. The other pair, at 2.52 Å distance (the shortest pair found), only resulted after Na insertion. These pairs pertain to the right and left peaks at -0.8 eV, respectively. The longest pair does not possess any bridging oxygens. The shortest pair, however, has two. Here we see again a kind of competition: even though one tungsten pair is much shorter, it does not result in a state much deeper in the gap. Apparently the bridging oxygens counteract. Configurations 7 and 8 are again borderline cases, involving several bridged W-W

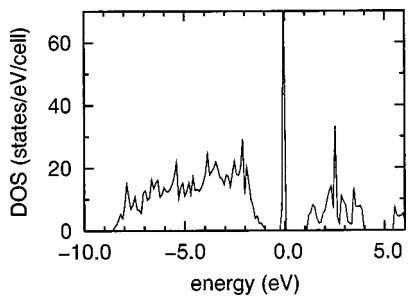

FIG. 17. GGA density of states of $AlWO_4$. Experimental atomic positions from Ref. 41 were used. The unit cell contains four formula units. The top of the valence bands is at zero.

pairs. Configuration 9 is again interesting: now there are three short tungsten pairs (2.81, 2.83, and 2.86 Å). Only the longest is not bridged by two oxygens (only by one) and this pair still carries the in-gap state. In configuration 10 the shortest W-W pair (2.65 Å) is bridged by only one oxygen and it carries the in-gap state at -1.2 eV.

Summarizing, the picture that emerged from the configurations with only oxygen removed needs to be qualified. In-gap states can also be induced by tungsten pairs bridged by two oxygens, but the tungsten atoms have to be significantly closer. Direct W-W interactions lead to lowering (from the conduction band) of a joint (filled) level into the gap. This is counteracted by indirect W-W interactions that are mediated by the oxygen atoms. The combined effect depends on the specific local geometry of (and around) the W-W pair.

IV. W^{5+} SPECIES IN CRYSTALLINE SYSTEMS

In the preceding section, two kinds of W^{5+} species were found: W^{5+}-W^{5+} pairs and magnetic W^{5+} ''atoms.'' In this section, contact is made with crystals incorporating W^{5+} species of both kinds.

Magnetic W^{5+} species are known to occur in the alkali metal containing hexachlorotungstates ($CsWCl_6$, $RbWCl_6$, $KWCl_6$, NH_4WCl_6, and $[N(C_2H_5)_4]WCl_6$).[39] In these systems the W^{5+} is surrounded by a nearly undistorted Cl octahedron.

Another system containing W^{5+} species is WOI_3.[40] There the W atoms are octahedrally coordinated by oxygen anions, however these octahedra are somewhat distorted. They are arranged in an edge-sharing geometry, in a way that results in W-W dimers with 3.10 Å intradimer distance. These W atoms are rather far apart, and in analogy to our amorphous samples where in-gap states were found for short W-W distances only, no in-gap states are expected. Indeed, WOI_3 is paramagnetic and has a small magnetic moment ($\sim 0.2\mu_B$).

Pairs of W^{5+} atoms [i.e., $(W\text{-}W)^{10+}$ species] have been observed in $AlWO_4$.[41] In its structure, chains of tungsten dimers with an intradimer distance of 2.61 Å occur. These pairs give rise to a filled state in the ''middle'' of the band gap (Fig. 17). This feature is reminiscent of our results for the oxygen-deficient samples, and lends support to the occurrence of $(W\text{-}W)^{10+}$ species in the amorphous solid.

Note that the GGA gap of Fig. 17 (~ 1 eV) is larger than the experimental gap of 0.35 eV. This is very unusual for a density-functional calculation. We speculate that the reason for this discrepancy is related to the imperfect stoichiometry of the samples used in Ref. 41 that could give rise to deep impurity levels. As the gap was determined from the activation energy for electrical conduction, it could be these states that are in fact seen in the experimental determination of the gap.

Similar tungsten pairs (also with 2.61 Å distance) have been observed in the similar compound $CrWO_4$.[42] Interestingly, the magnetism in this compound can be attributed entirely to the Cr^{3+} atoms, whereas the electrons from the W^{5+} species pair into a band well below the Fermi level.[43]

W^{5+} pairs also occur in $KH_3(W_2O_4F_6)$.[44] Like WOI_3, this compound contains W pairs in a geometry of edge-sharing (distorted) octahedra containing oxygen anions. However, in this compound the tungsten atoms are much closer at a distance of 2.62 Å. Hence, we expect a fully filled ''in-gap'' state, and indeed this compound was observed to be diamagnetic.

V. CONCLUSIONS

We summarize the results as follows.

(a) Amorphization of stoichiometric WO_3 results in an appreciable band-gap widening, because band broadening of the conduction band is frustrated. The occurrence of states in the gap is very unlikely.

(b) With the frustration of band broadening, the unoccupied valence-band states tend to localize. They do not localize on just one W atom but on a region encompassing several tungsten atoms.

(c) Doping by means of only alkali-metal (sodium) addition and oxygen deficiency are fundamentally different.

(d) Insertion of Na does not much affect the microscopic structure and results in a filling of (narrow) conduction-band states. Unpaired, somewhat delocalized, electrons can result (''W^{5+}'').

(e) Removal of oxygen triggers significant relaxations. In general, the occurrence of unpaired electrons seems unlikely. States deep in the gap can occur, when two tungsten atoms can approach rather close. These states are localized, i.e., confined close to the two tungsten atoms.

It has to be kept in mind that the above conclusions are based on calculations on small samples (i.e., the disorder is short range, and far from, e.g., a polycrystalline sample) that were generated by a very fast quench. These disadvantages are offset by the fact that our calculations are carried out from first-principles, and thus do not suffer from the approximations made in model and semiempirical calculations. Therefore, we hope they may provide a useful guide in the interpretation of experiments.

On the basis of our results, an alternative interpretation of the different experimental behavior of oxygen deficient and alkali-metal-intercalated films is conceivable. It was pointed out recently in Refs. 9 and 10 that oxygen-deficient films remain noncolored, whereas these should contain a significant number of W^{5+} species, and that these films can be colored by intercalation with small metal atoms (H,Li). This has been pointed out before (e.g., in Ref. 45), but the authors went a step further by noting that the coloration efficiency (upon alkali-metal intercalation) of the oxygen-deficient films depends linearly on oxygen deficiency. This is inconsistent with the picture of an IVCT transition between W^{6+}

and W^{5+} states, and the authors proposed a new IVCT mechanism based on a transition between W^{4+} and W^{5+} sites. W^{5+} sites would be less stable than W^{4+} sites and be created by ion intercalation. The amount of W^{4+} included in the film is determined by the oxygen shortage during film growth. So it is an inherent property of the film and should depend linearly on the oxygen shortage. This provides a mechanism to precondition the number of possible $W^{4+} \rightarrow W^{5+}$ transitions.

In light of our study, a W^{4+} species seems unlikely. However, oxygen shortage may lead to deep in-gap, completely filled states associated with a W-W bond [a $(W\text{-}W)^{10+}$ species]. Existence of such states is further supported by the occurrence of similar in-gap states in $AlWO_4$.[41] The presence of such pairs has also been suggested by Gérard *et al.*[45] to account for the absence of a W^{5+}-derived ESR signal and noncoloration in oxygen-deficient films. We suggest that, instead of a W^{4+}, these localized pairs are necessary for the occurrence of IVCT transitions. The pairs (brought about by oxygen deficiency) and the magnetic ''W^{5+}'' (caused by ion intercalation) should constitute important ingredients of the initial and final states of the IVCT transitions.

ACKNOWLEDGMENTS

Stimulating discussions with Dr. E.P. Boonekamp, Dr. T.J. Vink, and Professor L.F. Feiner are acknowledged. This work was part of the research program of the Stichting for Fundamenteel Onderzoek der Materie (FOM) with financial support from the Nederlandse Organisatie voor Wetenschappelijk Onderzoek (NWO).

[1] C.G. Granqvist, *Handbook of Inorganic Electrochromic Materials* (Elsevier, Amsterdam, 1995).
[2] A. Hjelm, C.G. Granqvist, and J.M. Wills, Phys. Rev. B **54**, 2436 (1996).
[3] B.W. Faughnan, R.S. Crandall, and P.M. Heyman, RCA Rev. **36**, 177 (1975).
[4] J.V. Gabrusenoks, P.D. Cikmach, A.R. Lusis, J.J. Kleperis, and G.M. Ramans, Solid State Ionics **14**, 25 (1984).
[5] V.V. Bryskin, Fiz. Tverd. Tela (Leningrad) **24**, 1110 (1982) [Sov. Phys. Solid State **24**, 627 (1982)].
[6] N.S. Hush, Prog. Inorg. Chem. **8**, 391 (1967).
[7] O.F. Schirmer, V. Wittwer, G. Baur, and G. Brandt, J. Electrochem. Soc. **124**, 749 (1977).
[8] S.K. Deb, Phys. Rev. B **16**, 1020 (1977).
[9] J.-G. Zhang, D.K. Benson, C.E. Tracy, S.K. Deb, A.W. Czanderna, and C. Bechinger, J. Electrochem. Soc. **144**, 2022 (1997).
[10] C. Bechinger, M.S. Burdis, and J.-G. Zhang, Solid State Commun. **101**, 753 (1997).
[11] R. Car and M. Parrinello, Phys. Rev. Lett. **55**, 2471 (1985).
[12] G. Kresse and J. Hafner, Phys. Rev. B **47**, 558 (1993); **49**, 14 251 (1994).
[13] G. Kresse and J. Furthmüller, Comput. Mater. Sci. **6**, 15 (1996).
[14] G. Kresse and J. Furthmüller, Phys. Rev. B **54**, 11 169 (1996).
[15] D. Vanderbilt, Phys. Rev. B **41**, 7892 (1990).
[16] G. Kresse and J. Hafner, J. Phys.: Condens. Matter **6**, 8245 (1994).
[17] S.G. Louie, S. Froyen, and M.L. Cohen, Phys. Rev. B **26**, 1738 (1982).
[18] R.D. King-Smith, M.C. Payne, and J.S. Lin, Phys. Rev. B **44**, 13 063 (1991).
[19] J.P. Perdew and A. Zunger, Phys. Rev. B **23**, 5048 (1981).
[20] D.M. Ceperley and B.J. Alder, Phys. Rev. Lett. **45**, 566 (1980).
[21] J.P. Perdew, J.A. Chevary, S.H. Voska, K.A. Jackson, M.R. Pederson, D.J. Singh, and C. Fiolhais, Phys. Rev. B **46**, 6671 (1992).
[22] G.A. de Wijs, P.K. de Boer, R.A. de Groot, and G. Kresse, Phys. Rev. B **59**, 2684 (1999).
[23] *Gmelin Handbuch der Anorganische Chemie, Wolfram Ergänzungsband B2, Oxide 1979* (Springer, Berlin, 1979).
[24] M.S. Mattsson, Phys. Rev. B **58**, 11 015 (1998).
[25] H.J. Monkhorst and J.D. Pack, Phys. Rev. B **13**, 5188 (1976).
[26] P.E. Blöchl, O. Jepsen, and O.K. Andersen, Phys. Rev. B **49**, 16 223 (1994).
[27] The number of possible configurations with bond angles between θ and $\theta + d\theta$ is proportional to $\sin(\theta)d\theta = -d(\cos(\theta))$.
[28] The distribution was calculated observing the minimum-image convention. In principle, problems concerning the interpretation already arise beyond half the box length (i.e., beyond 3.74 Å). However, that does not much affect the basic features.
[29] N.-L. Vannerberg, Prog. Inorg. Chem. **4**, 125 (1962).
[30] Note that a superoxide, having one unpaired electron, is not likely to be found in our calculation, where we have not included spin.
[31] Peroxidelike oxygen dimers have been observed with STM on the (001) surface of $Na_{0.65}WO_3$. [F.H. Jones, K.H. Rawlings, J.S. Foord, P.A. Cox, R.G. Egdell, and J.B. Pethica, J. Chem. Soc. Chem. Commun. **1995**, 2419]. Here the oxygens in the Na/O surface plane dimerize to form O-O bonds with an intradimer separation of 2.2 Å. The large intradimer separation already shows that such O-O species are quite different from those found in our simulation that are embedded in a matrix of bulk WO_3.
[32] B.O. Loopstra and P. Boldrini, Acta Crystallogr. **21**, 158 (1966); B.O. Loopstra and H.M. Rietveld, Acta Crystallogr., Sect. B: Struct. Crystallogr. Cryst. Chem. **25**, 1420 (1969).
[33] T. Horie, K. Kawabe, and T. Iwai, Ann. Rep. Sci. Works Fac. Sci. Osaka Univ. **4**, 45 (1956).
[34] T. Iwai, J. Phys. Soc. Jpn. **15**, 1596 (1960).
[35] E. Salje, Opt. Commun. **24**, 231 (1978).
[36] R.J. Bell and P. Dean, in *Amorphous Materials*, edited by R.W. Douglas and B. Ellis (Wiley, New York, 1972), p. 443.
[37] This is an oxygen-deficient structure. This only affects in-gap states that do not matter in the general discussion of the conduction-band states.
[38] The only possibly similar case is configuration 2, where a band was separated from the other conduction bands already in the stoichiometric amorphous sample. However, this band was separated from the valence band by a gap of 1.8 eV and not much more localized than many other conduction-band states.
[39] W. Eichler and H.-J. Seifert, Z. Anorg. Allg. Chem. **431**, 123 (1977).

[40] B. Krebs, C. Brendel, and H. Schäfer, Z. Anorg. Allg. Chem. **553**, 127 (1987).
[41] J.P. Doumerc, M. Vlasse, M. Pouchard, and P. Hagenmuller, J. Solid State Chem. **14**, 144 (1975).
[42] M. Vlasse, J.-P. Doumerc, P. Peshev, J.-P. Chaminade, and M. Pouchard, Rev. Chim. Miner. **13**, 451 (1976).
[43] J.-P. Doumerc, S. Angelov, F. Ménil, and M. Pouchard, Mater. Res. Bull. **11**, 673 (1976).
[44] R. Mattes and K. Mennemann, Z. Anorg. Allg. Chem. **437**, 175 (1977).
[45] P. Gérard, A. Deneuville, and R. Courths, Thin Solid Films **71**, 221 (1980).